Exclusive pion production from few nucleon systems in the region of the Δ_{1232} resonance

K. M. Furutani,* W. R. Falk, H. Guan, and J. R. Campbell
Department of Physics, University of Manitoba, Winnipeg, Manitoba, Canada R3T 2N2

F. A. Duncan†
Department of Physics, University of British Columbia, Vancouver, British Columbia, Canada V6T 2A6

P. L. Walden and S. Yen
TRIUMF, Vancouver, British Columbia, Canada V6T 2A3

G. M. Huber‡ and R. D. Bent
Indiana University Cyclotron Facility, Bloomington, Indiana 47405

G. J. Lolos
Department of Physics, University of Regina, Regina, Saskatchewan, Canada S4S 0A2

E. Korkmaz§
Department of Physics, University of Alberta, Edmonton, Alberta, Canada 6TG 2N5

A. Trudel
Department of Physics, Simon Fraser University, Vancouver, British Columbia, Canada V6T 2A6

A. Celler
Department of Physics, University of Western Ontario, London, Ontario, Canada T6G 2N5
(Received 10 May 1994)

Angular distributions of the differential cross sections and analyzing powers have been measured for the ^{3}He$(\vec{p},\pi^+)^4$He and ^{4}He$(\vec{p},\pi^+)^5$He reactions at proton bombarding energies between 240 and 507 MeV. These new results provide a comprehensive set of data spanning the region of the Δ_{1232} resonance and are compared with a phenomenological model that incorporates the amplitudes for the $pp \rightarrow d\pi^+$ reaction, and with calculations from a microscopic (p,π^+) model. A ^{5}He final state interaction calculation based upon the low energy $n+\alpha$ elastic phase shifts indicates that the ^{4}He$(p,\pi^+)^5$He spectra are nearly independent of pion angle and proton energy. Comparisons made with the time reversed charge symmetric reaction ^{3}H$(n,\pi^-)^4$He reaction indicate substantial Coulomb effects are still present at 300 MeV.

PACS number(s): 25.40.Qa, 24.70.+s, 21.45.+v

I. INTRODUCTION

Proton induced nuclear pion production provides a unique probe of pion interactions in nuclei. Investigation of the exclusive nuclear pion production reaction $A(p,\pi^+)A+1$ was initiated over two decades ago with the pioneering studies at Uppsala [1]. Several reviews of the subject [2] give an excellent survey of the data and theory up to the late 1970s and early 1980s and many of the questions raised in Ref. [3] remain open questions today.

Because of the relatively large mass difference between the proton and pion, a large momentum is transferred to the final state nucleus. This momentum transfer is typically several times the nuclear Fermi momentum. How the nucleus absorbs this large momentum transfer is a central problem to understanding $A(p,\pi^+)A+1$ reactions. In the case of the lowest-order pionic stripping, or one nucleon model, the cross section is proportional to the Fourier transform of the radial neutron wave function. To lowest order then, the (p,π^+) reaction probes the high momentum components of the nuclear wave function. However, such a description results in zero analying powers and the observed nonzero analyzing powers of $A(p,\pi^+)A+1$ reactions precludes a single nucleon

*Present address: Department of Physics, York University, Toronto, ON, Canada M3J 1P3.
†Present address: Department of Physics, University of Maryland, College Park, MD 20742.
‡Present address: Department of Physics, University of Regina, Regina, SK, Canada S4S 0A2.
§Present address: Department of Physics, University of Northern British Columbia, Prince George, BC, Canada V2L 5P2.

mechanism alone [2]. Higher-order multinucleon effects result in substantial redistribution and sharing of the large momentum transfer and permit nonzero values of the analyzing powers.

Pion production has been studied theoretically in terms of both one nucleon and two nucleon models [2–4]. At the one nucleon level, higher-order effects are included by distortions of the proton and pion wave functions calculated from proton or pion optical potentials. The on-shell wave functions are obtained by fitting the optical potential parameters to the elastic data and then extrapolated off-shell according to the model description of the (p,p) or (π^+,π^+) interaction. Pion production reactions are quite naturally sensitive to this extrapolation, which therefore provides valuable insight into the validity of the optical model assumptions. At the two nucleon level, detailed microscopic calculations include some of the higher-order processes in an explicit way [4,5]. However, the models differ in their treatment of these effects and which diagrams they include in the calculations. Frequently, as a result, the models have been applied only to selective cases for which they seemed most appropriate. Within these limited areas of application each of these models has had a measure of success. None has been able to describe a large body of data. Moreover, the models have demonstrated a significant sensitivity to distortions and other parameters in the calculations.

In light of these shortcomings of the microscopic calculations, emphasis has shifted in recent years to qualitative elucidation of the role of the elementary $NN \rightarrow NN\pi$ processes in the $A(p,\pi^+)A+1$ reactions. Strong empirical evidence exists which suggests that the exclusive (p,π^+) reaction is mediated by a process, or processes, like the elementary $pp \rightarrow d\pi^+$ reaction [6]. Indeed, Korkmaz [7] and Huber [8] have used a kinematical transformation of the $pp \rightarrow d\pi^+$ analyzing powers to the nuclear frame to demonstrate striking similarities in these reactions. The similarity of the $A(p,\pi^+)A+1$ analyzing power energy dependence to the $pp \rightarrow d\pi^+$ reaction in the region of the Δ_{1232} is strong evidence of an underlying $NN \rightarrow N\Delta \rightarrow NN\pi^+$ process. Recent impulse model calculations of Kurath [9] and Falk [10], which use $pp \rightarrow d\pi^+$ amplitudes as a description of the pion production mechanism in the nucleus, have met with some qualitative success.

Both the impulse and microscopic calculations require substantial study before the details of the reaction mechanism can be understood. This requires investigation of kinematical and dynamical parameters of the (p,π^+) reaction over a broad range of values encompassing the Δ_{1232} resonance. In an effort to achieve this understanding we address pion production in few body nuclei, specifically the $^3\mathrm{He}(\vec{p},\pi^+)^4\mathrm{He}$ and $^4\mathrm{He}(\vec{p},\pi^+)^5\mathrm{He}$ reactions [11]. Such systems have relatively simple nuclear structure and, moreover, should make the multinucleon aspects of the calculation simpler. Indeed, a microscopic model calculation of Alons *et al.* [5] uses the helium system as a test reaction. However, to study the dynamics of the reaction mechanism more data are required, in particular, the energy dependence of the analyzing powers.

There presently exist data for the differential cross sections for these reactions at several energies: near threshold for $^3\mathrm{He}(p,\pi^+)^4\mathrm{He}$ [12,13] and $^4\mathrm{He}(p,\pi^+)^5\mathrm{He}$ [14]; at 415 and 716 MeV for $^3\mathrm{He}(p,\pi^+)^4\mathrm{He}$ [15]; at 800 MeV for $^3\mathrm{He}(p,\pi^+)^4\mathrm{He}$ and $^4\mathrm{He}(p,\pi^+)^5\mathrm{He}$ [16]; and two measurements carried out at a single energy and angle for $^3\mathrm{He}(p,\pi^+)^4\mathrm{He}$ [17]. The proton bombarding energy of 415 MeV corresponds approximately to the energy where a nucleon inside the nucleus may be excited to a Δ, i.e., $E_{\mathrm{c.m.}} - m_{\mathrm{target}} \approx m_\Delta$. Measurements of the analyzing powers for the $^3\mathrm{He}(\vec{p},\pi^+)^4\mathrm{He}$ and $^4\mathrm{He}(\vec{p},\pi^+)^5\mathrm{He}$ reactions are less extensive than those for the cross sections. For the $^3\mathrm{He}(\vec{p},\pi^+)^4\mathrm{He}$ reaction there are analyzing power data at 178 and 198 MeV from the Indiana University Cyclotron Facility (IUCF) [12] and at 800 MeV for both the $^3\mathrm{He}(\vec{p},\pi^+)^4\mathrm{He}$ and $^4\mathrm{He}(\vec{p},\pi^+)^5\mathrm{He}$ reactions from LAMPF [16]. There remains a large gap between threshold and 800 MeV in the region of the Δ_{1232} resonance. It was in this region that the present measurements were made.

II. EXPERIMENT

A. Polarized proton beam

Two separate experiments were carried out, one for the $^3\mathrm{He}(\vec{p},\pi^+)^4\mathrm{He}$ reaction and one for the $^4\mathrm{He}(\vec{p},\pi^+)^5\mathrm{He}$ reaction (referred to as EXP1 and EXP2, respectively). These experiments were performed in the proton hall of the TRIUMF laboratory using the medium resolution spectrometer (MRS). Achromatic polarized proton beams with typical momentum resolutions of $\Delta p/p \approx 0.2\%$ were extracted from the TRIUMF cyclotron with kinetic energies of 300, 416, and 507 MeV for the $^3\mathrm{He}(\vec{p},\pi^+)^4\mathrm{He}$ experiment and 240, 300, 400, and 500 MeV for the $^4\mathrm{He}(\vec{p},\pi^+)^5\mathrm{He}$ experiment. These beams were incident on a liquid helium target (^{3}He in EXP1 and ^{4}He in EXP2) with intensities ranging from 5 to 40 nA, and with typical polarizations of 70%. Calibration measurements were also carried out in both experiments at the highest proton energies (507 and 500 MeV) using the $pp \rightarrow d\pi^+$ reaction.

The number of beam protons, N_p, was measured using an in-beam polarimeter (IBP) and a secondary emission monitor (SEM), positioned upstream and downstream of the target, respectively. These two instruments were calibrated in previous experiments using a Faraday cup and provided independent measurements of the beam intensity which agreed to within 3% for EXP1 and 5% for EXP2. Beam polarization, P, was measured using the IBP. Systematic uncertainties in the beam polarization are dominated by the uncertainty of the $\vec{p}p \rightarrow pp$ analyzing powers (determined using SAID [18]) and estimated to be about 2%.

III. LIQUID HELIUM TARGET

The University of Manitoba–TRIUMF liquid helium target [19] was extensively refurbished and upgarded in preparation for these experiments. The cryostat con-

tained two internal two targets: a dummy cell and a target cell, and an externally mounted CH_2/ZnS screen. A lifting mechanism permitted any of these targets to be positioned in the beam line, and a rotation mechanism allowed selection of the target angle. The helium cell was about 44 mm in diameter and 11 mm thick comprising a brass frame with indium sealed 25.4 μm thick stainless steel windows. Mounted on this brass frame were two calibrated germanium resistors [20] for temperature measurement. From these temperature measurements the target density ρ was determined [21].

The target was maintained at a stable temperature of about 1.9±0.2 K, which corresponded to densities of about 78 mg/cm^3 for ^{3}He and 146 mg/cm^3 for ^{4}He with uncertainties of less than 3%. Comparisons of proton elastic scattering ^{3}He$(p,p)^3$He and ^{4}He$(p,p)^4$He with previous measurements [22,23] confirmed the calculated target densities.

A. Spectrometer

Scattered pions were tracked by the MRS spectrometer [24]. The MRS is a vertical bend quadrupole-dipole, 1.6 GeV/c spectrometer instrumented with a front end multiwire horizontal drift chamber (FEC) at the entrance to the quadrupole, and two vertical drift chambers (VDC) and a scintillator hodoscope at the exit of the dipole. Good track reconstruction is provided by the chamber information, and particle identification from particle time of flight and energy loss in the scintillator hodoscope. The MRS was designed for proton scattering experiments, and in order to understand its performance as a pion spectrometer a Monte Carlo study was undertaken. Particle rays were traced through the spectrometer containing all the physical constraints of the system and the absorbers in the target area and in the various windows. The Monte Carlo calculations included the effects of energy loss, straggling, multiple scattering and pion decay, i.e., $\pi^+ \rightarrow \mu^+ + \bar{\nu}_\mu$. Muons from pions which decay inside the dipole are lost to the detector system; those from pions decaying after the dipole are often detected in the following detector stack. As discussed in Sec. III, trajectories which did not reconstruct back to the target were rejected. Results of this study indicate that the MRS can be represented by an effective pion survival length, L_π. The fraction of pions which survive transit through the spectrometer is given by the expression

$$\eta_\pi = \exp\left\{\frac{-m_\pi L_\pi}{p_\pi c\tau}\right\},$$

where τ is the mean lifetime (2.603×10^{-8} s), m_π the mass (139.57 MeV/c^2), and p_π the momentum (in MeV/c) of the pion. The pion survival length of the MRS determined by the Monte Carlo calculations was

$$L_\pi = (11.10 \pm 0.03)m,$$

and represents a good parameterization for pion energies greater than about 50 MeV.

IV. ANALYSIS

The nonbend plane acceptance of the MRS at the target, $g(x)$, was calibrated using the $pp \rightarrow d\pi^+$ reaction by stepping the beam horizontally across a thin solid CH_2 target. These experimental results, measured at two MRS angles of 28° and 122°, together with corresponding Monte Carlo calculations previously described, are shown in Fig. 1(b). Generally good agreement between the measurements and calculations is observed in a central region (±6 mm), with increasing divergence in the tails of the distributions. Fortunately, these tails have little effect on the current experiments.

The target profile $f(x)$—the intersection of the beam with the target—was calculated assuming a uniform proton beam distribution of finite width ($\approx$ 4 mm); this is trapezoidal in shape, as indicated in Fig. 1(a), and results in the typical profiles shown in Fig. 1(b). The effective target length was then calculated from the target profile $f(x)$ weighted with the nonbend plane acceptance, $g(x)$, of the MRS as follows:

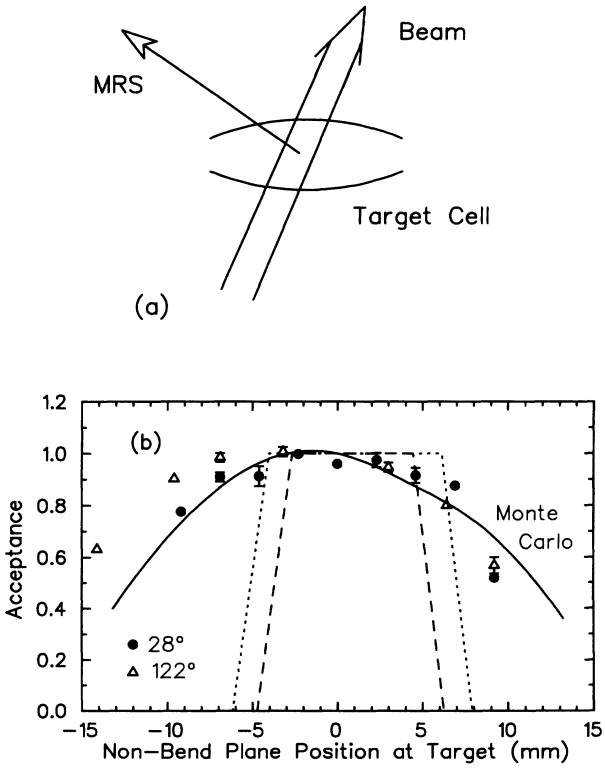

FIG. 1. (a) Intersection of proton beam of finite width with the target. (b) The nonbend plane acceptance of the MRS determined using the $pp \rightarrow d\pi^+$ reaction at 500 MeV for the two laboratory angles of 28° and 122°. The solid curve is the corresponding result from a Monte Carlo calculation. The dashed curves are typical target profiles projected onto the MRS acceptance. They depend on the target angle and MRS angle.

$$L_t = \int f(x)g(x)dx.$$

Effective target lengths calculated with the two different experimental acceptances differed by about 0.5% for the narrower profile, and 1% for the wider profile. Cross section measurements for the ^{3}He$(\vec{p},\pi^+)^4$He reaction at a fixed MRS scattering angle and different target angles were carried out and confirmed the validity of the above procedure for calculating the effective target length. Sensitivity of this calculation to uncertainties in the beam width and position results in an estimated error of 3%.

The momentum acceptance of the MRS, η_{focal}, was determined by measuring the yield from the $pp \rightarrow d\pi^+$ reaction as a function of focal plane position. Results of the Monte Carlo calculation compared well with these measurements in the central region of the focal plane. During the experiment the pion peak was always positioned in the region where η_{focal} was close to unity and nearly constant.

Pions were identified from their time of flight through the spectrometer and their energy loss in the scintillator hodoscope at the exit of the dipole. A master trigger was formed from events identified as pions in coincidence with signals in the first plane of VDC1 and one of the FEC planes. The trigger was subsequently inhibited while all the electronics were read out. An estimate for the efficiency of a chamber could be made since sufficient information was written to tape. For example, the FEC chamber efficiency was determined as follows:

$$\eta_{\text{FEC}} = \frac{N_{\text{VDC1}\cdot\text{VDC2}\cdot\text{FEC}}}{N_{\text{VDC1}\cdot\text{VDC2}}},$$

where $N_{\text{VDC1}\cdot\text{VDC2}\cdot\text{FEC}}$ is the number of events where all the chambers have properly decoded signals, and $N_{\text{VDC1}\cdot\text{VDC2}}$ is the number of events where both VDC's have properly decoded signals. A similar formula was used for each of the VDC's. The FEC efficiency depends on the FEC rate, and the beam current was maintained at a level where the FEC rate was below 1 MHz, such that efficiencies were typically $\geq$70%. Because of the low rate environment of the VDC's, their efficiencies were nearly always greater than 90%. A total chamber efficiency, η_{chmb}, was calculated from the product of the individual chamber efficiencies and ranged from 70% to nearly unity depending on the FEC rate. The livetime of the MRS data acquisition system was estimated from the ratio of the computer busy and master trigger rates. It was also checked against a random pulser whose rate was proportional to the incident beam current. The statistical errors of the chamber efficiency and the live time were determined as described in [25].

Using the information from the wire chamber coordinates the pion trajectories were reconstructed. Tracks which did not reconstruct as originating from the target were rejected. By varying the cuts on the reconstructed coordinates, the uncertainty in the yield due to the placement of software cuts was estimated at about 3%.

The spectrometer solid angle was determined in a different manner for each of the two experiments. For ^{3}He$(p,\pi^+)^4$He (and the associated $pp \rightarrow d\pi^+$ calibration reaction), cuts were placed on the acceptance at the entrance to the spectrometer via the FEC and the solid angle determined geometrically. This geometrical method resulted in a relative point-to-point error of 4% and an overall systematic error of 3%. For ^{4}He$(p,\pi^+)^5$He, the highest possible statistics were required for extraction of the broad ^{5}He resonance, and therefore no cuts on the FEC could be tolerated. A method, similar to that used in previous analyses of (p,π^+) experiments [26], with no cut on the FEC, was employed. By keeping the ratio of the quadrupole field to dipole field (Q/D ratio) constant, the optics of the MRS are kept constant, and therefore so is the solid angle of the MRS. Nevertheless, small variations in the Q/D ratio did occur, requiring detailed knowledge of the associated solid angle dependence. The dependence of the solid angle on Q/D, extrapolated to open cuts on the FEC, was determined using the $pp \rightarrow d\pi^+$ reaction. In the vicinity of the value used for EXP2, $Q/D \approx 0.48$, it was found that

$$\Delta\Omega = 7.69Q/D - 1.07 \text{ (msr)} .$$

From this relation the solid angle is observed to be quite sensitive to small changes in Q/D ratio, namely,

$$\frac{\delta\Delta\Omega}{\Delta\Omega} \approx 1.4\frac{\delta Q/D}{Q/D}.$$

This experimental result was confirmed via Monte Carlo calculations. The variations in the Q/D ratio thoughout EXP2 were such that the resulting point-to-point uncertainties were no more than 2%. An overall systematic uncertainty was estimated at 6% from the $pp \rightarrow d\pi^+$ calibration measurements.

A. Spectra

Typical experimental ^{3}He(p,π^+) and ^{4}He(p,π^+) spectra are shown in Figs. 2 and 3. In the case of ^{3}He$(p,\pi^+)^4$He the pion peak from the ^{4}He ground state is cleanly resolved from the ^{4}He excited states (which start at about 20 MeV excitation) as observed in the 18.4° spectrum. Background from these spectra was subtracted using a linear estimation in the vicinity of the peak, and the net counts integrated. In the case of ^{4}He$(p,\pi^+)^5$He the recoil ^{5}He is an unbound $n+\alpha$ resonance ($Q \approx 0.9$ MeV and FWHM$\approx$ 0.6 MeV). Background spectra were obtained from dummy cell runs performed at several angles for each proton bombarding energy. These background spectra exhibit cross sections which were found to be nearly linear in momentum and only weakly dependent on angle, consistent with the observations of Crawford *et al.* [27] and Krasnov *et al.* [28]. For each proton energy the background was parametrized in terms of a Legendre polynomial series and subtracted from the ^{4}He(p,π^+) spectra by normalizing to the number of integrated counts between channels 3000 to 4000. The resulting spectra were then integrated from 0 to 4.44 MeV excitation of ^{5}He. This upper limit was selected to facilitate comparison with already published

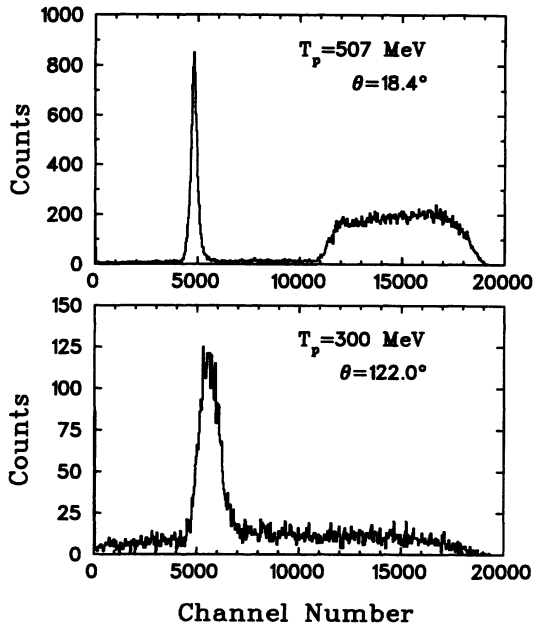

FIG. 2. Typical experimental ^{3}He(p,π^+) spectra. The pion peak from the ^{4}He ground state is observed to be cleanly separated from the ^{4}He excited states (which start at approximately 20 MeV excitation) in the 18.4° spectrum. The excitation energy per channel is approximately 3.5 and 1.0 keV/channel for the 18.4° and 122° spectra, respectively.

data [14]. To best understand the shape of the spectra for the ^{4}He(p,π^+) measurements, a final state interaction calculation was performed, and this is discussed in Sec. IV D.

B. Cross sections

The spin-dependent cross section was calculated according to the expression

$$\frac{d\sigma}{d\Omega_{\rm c.m.}} = \frac{Y_\pi}{(\eta_{\rm chmb}\eta_{\rm live}N_p)(\eta_\pi\eta_{\rm focal}\eta_{\rm loss}\rho L_t\Delta\Omega)}\frac{d\Omega_{\rm lab}}{d\Omega_{\rm c.m.}}.$$

The rate-dependent efficiencies (the wire chamber efficiency, $\eta_{\rm chmb}$, and the live time of the data acquisition system, $\eta_{\rm live}$) were determined separately for the up and down polarizations. The rate-independent efficiencies comprise the pion survival fraction, η_π, the momentum accpetance, $\eta_{\rm focal}$, and the reaction losses, $\eta_{\rm loss}$, of the MRS. The differential cross section is then given by

$$\frac{d\sigma}{d\Omega} = \frac{P(\downarrow)d\sigma/d\Omega(\uparrow) + P(\uparrow)d\sigma/d\Omega(\downarrow)}{P(\uparrow)+P(\downarrow)},$$

where $\uparrow$ and $\downarrow$ refer to the direction of the incident beam polarized in the *up* and *down* directions, respectively. These cross sections are shown in Figs. 4 and 5, and the numerical data in Tables I and II.

A statistical and relative point-to-point uncertainty of each datum is quoted in Tables I and II of about 5% for the ^{3}He$(p,\pi^+)^4$He data and 6% for ^{4}He$(p,\pi^+)^5$He.

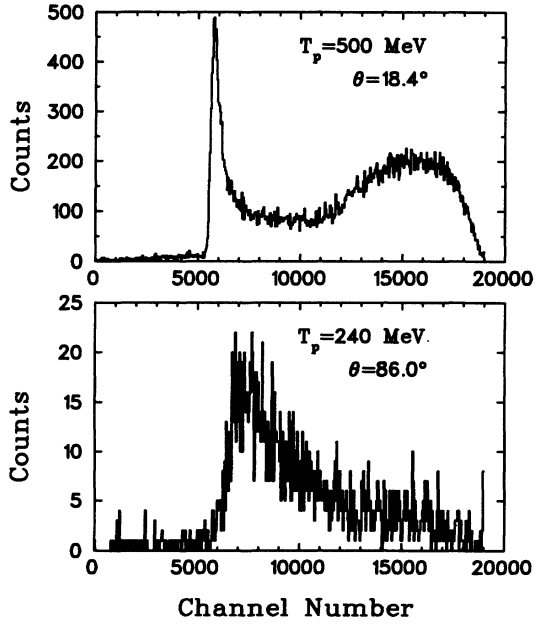

FIG. 3. Typical experimental ^{4}He(p,π^+) spectra. The recoil ^{5}He is an unbound $n+\alpha$ resonance ($Q\approx 0.9$ MeV and FWHM$\approx$ 0.6 MeV). The excitation energy per channel is approximately 3.5 and 0.66 keV/channel for the 18.4° and 86.0° spectra, respectively.

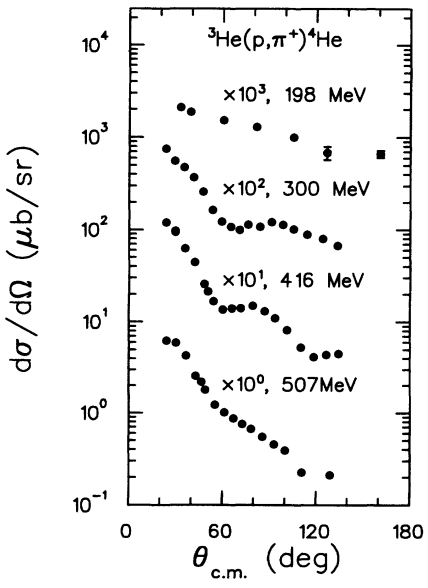

FIG. 4. Differential cross sections for the ^{3}He$(\vec{p},\pi^+)^4$He reaction. The data at 198 MeV are from Kehayias *et al.* [12]. The errors bars comprising the statistical and relative uncertainties added in quadrature are typically ±5%. In addition, there is an overall systematic error, not shown, of ±5%.

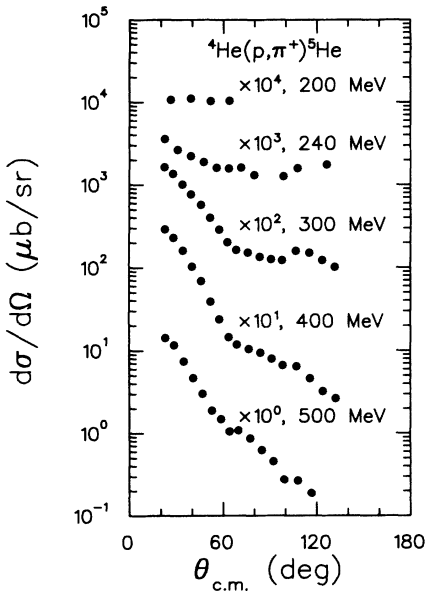

FIG. 5. Differential cross sections for the ^{4}He$(\vec{p},\pi^+)^5$He reaction. The 200 MeV data are from LeBornec *et al.* [14]. The errors bars comprising the statistical and relative uncertainties added in quadrature are typically ±6%. In addition, there is an overall systematic error, not shown, of ±8%.

The overall systematic uncertainty is about 5% for the ^{3}He$(p,\pi^+)^4$He data and 8% for ^{4}He$(p,\pi^+)^5$He.

Independent checks of all calibrations and data extraction procedures were made by comparison with the previously measured $pp \rightarrow d\pi^+$ cross sections and elastic scattering on ^{3}He [22] and ^{4}He [23]. These various comparisons were consistent within the overall errors.

C. Analyzing powers

In the Ann Arbor convention [29], the analyzing power is given by the expression

$$A_{N0} = \frac{d\sigma/d\Omega(\uparrow) - d\sigma/d\Omega(\downarrow)}{P(\downarrow)d\sigma/d\Omega(\uparrow) + P(\uparrow)d\sigma/d\Omega(\downarrow)}.$$

Note that in the older Madison convention [30] the analyzing power is denoted A_y. The measured analyzing powers for the ^{3}He$(\vec{p},\pi^+)^4$He and ^{4}He$(\vec{p},\pi^+)^5$He reactions are shown in Figs. 6 and 7. Uncertainties in the analyzing powers due to the rate-dependent efficiencies and extraction of the peak area above background were typically ±0.04. It was found for ^{4}He$(p,\pi^+)^5$He that the analyzing powers were relatively insensitive to the method of peak extraction.

D. Final state interaction

To understand the shape of the spectra for the ^{4}He(p,π^+) experiment a final state interaction (FSI) calculation was carried out. The FSI calculation is based on the low-energy $n+\alpha$ elastic scattering phase shifts fit by Bond and Firk [31]. A ^{5}He wave function $\psi_j(k,r)$ was written in terms of these phase shifts by Germond and Wilkin [32] where j is the total angular momentum of the $n+\alpha$ system in a relative P state (i.e., $P_{1/2}$ or $P_{3/2}$) and k and r are the relative momentum and space coordinates, respectively. In Fig. 8 the $P_{1/2}$ and $P_{3/2}$ wave functions are shown for $k = 0.2$ fm^{-1} and 0.4 fm^{-1}. One should note the similarity in the shape of the wave functions for $r \leq 2$ fm. The FSI is usually assumed to be

TABLE I. Cross sections and analyzing powers for the ^{3}He$(\vec{p},\pi^+)^4$He reaction. The errors in the cross sections comprise the statistical and relative uncertainties added in quadrature and are typically ±5%. In addition, there is an overall systematic uncertainty (not shown in the tables) of ±5%. The analyzing powers are subect to an overall systematic uncertainty (not shown in the tables) of ±2%.

T_p = 507 MeV			T_p = 416 MeV			T_p = 300 MeV		
$\theta_{c.m.}$ (deg)	$d\sigma/d\Omega$ (μb/sr)	A_{N0}	$\theta_{c.m.}$ (deg)	$d\sigma/d\Omega$ (μb/sr)	A_{N0}	$\theta_{c.m.}$ (deg)	$d\sigma/d\Omega$ (μb/sr)	A_{N0}
24.25	6.25±0.19	0.424±0.040	23.79	11.94±0.56	0.562±0.032	23.37	7.52±0.34	0.331±0.035
30.20	5.95±0.31	0.250±0.055	29.63	9.41±0.43	0.550±0.031	29.13	5.57±0.26	0.463±0.033
36.61	4.29±0.18	0.053±0.039	29.63	9.71±0.45	0.526±0.037	35.33	4.76±0.22	0.330±0.037
42.88	2.56±0.11	−0.174±0.042	35.96	6.26±0.28	0.454±0.036	41.46	3.70±0.17	0.338±0.038
46.64	2.195±0.098	−0.226±0.041	42.18	4.42±0.20	0.354±0.035	47.48	2.60±0.11	0.129±0.036
49.08	1.792±0.082	−0.288±0.042	48.30	2.58±0.11	0.211±0.036	53.45	1.644±0.073	−0.095±0.038
55.19	1.226±0.054	−0.181±0.040	50.69	2.14±0.11	0.135±0.048	59.35	1.225±0.055	−0.402±0.032
61.17	1.011±0.053	0.129±0.059	54.31	1.681±0.070	−0.057±0.035	65.17	1.074±0.050	−0.548±0.034
67.04	0.869±0.049	0.314±0.062	60.21	1.364±0.059	−0.073±0.038	70.79	0.994±0.046	−0.544±0.033
72.74	0.757±0.037	0.567±0.041	66.04	1.403±0.061	0.138±0.038	76.36	1.138±0.051	−0.343±0.036
78.32	0.669±0.034	0.738±0.036	71.71	1.408±0.063	0.299±0.038	83.96	1.078±0.047	−0.115±0.037
85.82	0.548±0.027	0.756±0.030	79.45	1.504±0.068	0.475±0.037	91.31	1.219±0.053	0.017±0.035
93.26	0.456±0.021	0.709±0.030	86.97	1.312±0.064	0.632±0.033	98.44	1.139±0.050	0.068±0.037
100.34	0.391±0.018	0.409±0.040	93.74	1.104±0.052	0.652±0.031	105.39	1.013±0.044	0.031±0.036
111.00	0.225±0.013	0.031±0.073	101.39	0.816±0.038	0.542±0.034	114.01	0.884±0.039	−0.076±0.037
129.02	0.211±0.014	−0.744±0.062	110.12	0.530±0.024	0.200±0.038	124.13	0.797±0.036	−0.250±0.037
			118.48	0.414±0.019	−0.368±0.039	133.81	0.669±0.031	−0.613±0.028
			126.52	0.437±0.024	−0.871±0.031			
			134.32	0.450±0.025	−1.050±0.022			

an enhancement of phase space, and this three-particle differential phase space is given by [33]

$$\frac{dR_3}{d\Omega_\pi dp_\pi} = \frac{\pi p_\pi^2}{2E_\pi} \frac{\sqrt{[E_{n\alpha}^2 - (m_n + m_\alpha)^2][E_{n\alpha}^2 - (m_n - m_\alpha)^2]}}{2E_{n\alpha}^2},$$

where p_π and E_π are the pion momentum and energy in the laboratory frame and the $n + \alpha$ invariant mass is given by

$$E_{n\alpha} = m_n + m_\alpha + E_x.$$

Since the excitation energies E_x considered here are of the order of a few MeV, the $n + \alpha$ relative momentum k may be related to the excitation energy in a nonrelativistic approximation

$$k = \frac{\sqrt{2\mu E_x}}{\hbar c},$$

where μ is the reduced mass (in MeV/c^2) of the $n + \alpha$ system.

TABLE II. Cross sections and analyzing powers for the ^{4}He$(\vec{p}, \pi^+)^5$He reaction. The errors in the cross sections comprise the statistical and relative uncertainties added in quadrature and are typically ±6%. In addition, there is an overall systematic uncertainty (not shown in the tables) of ±8%. The analyzing powers are subect to an overall systematic uncertainty (note shown in the tables) of ±2%.

T_p = 500 MeV			T_p = 400 MeV		
$\theta_{\text{c.m.}}$ (deg)	$d\sigma/d\Omega$ (μb/sr)	A_{N0}	$\theta_{\text{c.m.}}$ (deg)	$d\sigma/d\Omega$ (μb/sr)	A_{N0}
23.02	14.23±0.92	0.576±0.052	22.60	29.1±1.6	0.421±0.051
28.66	11.64±0.57	0.215±0.044	28.27	23.0±1.3	0.491±0.041
34.82	7.41±0.36	−0.003±0.044	34.27	16.14±0.67	0.497±0.037
40.86	4.68±0.23	−0.057±0.047	40.21	10.27±0.64	0.326±0.062
46.79	3.02±0.15	−0.269±0.047	46.08	6.90±0.35	0.261±0.046
52.67	1.89±0.10	−0.416±0.048	51.93	3.90±0.29	0.045±0.088
58.48	1.487±0.092	−0.283±0.066	57.67	2.37±0.19	−0.132±0.095
64.18	1.052±0.053	0.051±0.053	63.33	1.448±0.075	−0.363±0.047
69.82	1.084±0.058	0.430±0.051	68.92	1.179±0.059	−0.177±0.047
77.42	0.865±0.046	0.616±0.046	76.51	1.048±0.054	0.158±0.049
84.85	0.625±0.034	0.697±0.044	83.99	0.948±0.051	0.396±0.046
92.19	0.455±0.024	0.650±0.044	91.25	0.794±0.048	0.615±0.055
99.25	0.274±0.015	0.557±0.049	98.34	0.665±0.041	0.735±0.048
108.02	0.267±0.014	0.325±0.052	107.15	0.643±0.035	0.664±0.041
116.50	0.187±0.009	−0.154±0.072	115.69	0.461±0.024	0.438±0.045
			123.95	0.323±0.016	0.055±0.048
			132.02	0.264±0.014	−0.443±0.048
	T_p = 300 MeV			T_p = 240 MeV	
22.38	16.35±0.80	0.300±0.041	22.66	3.57±0.20	0.027±0.056
27.95	13.63±0.72	0.362±0.051	30.70	2.65±0.15	−0.030±0.059
33.92	10.07±0.53	0.277±0.049	39.11	2.24±0.13	−0.133±0.060
39.38	7.69±0.42	0.326±0.061	47.39	1.89±0.11	−0.352±0.055
45.69	5.71±0.32	0.343±0.051	55.58	1.62±0.11	−0.581±0.051
51.52	4.02±0.24	0.165±0.059	63.56	1.58±0.10	−0.795±0.041
57.21	2.88±0.15	−0.133±0.048	71.40	1.62±0.11	−0.895±0.034
62.87	2.03±0.11	−0.422±0.045	80.12	1.312±0.092	−0.874±0.044
68.41	1.630±0.092	−0.670±0.038	98.83	1.263±0.072	−0.614±0.043
76.01	1.518±0.086	−0.791±0.028	107.77	1.585±0.094	−0.629±0.056
83.51	1.348±0.074	−0.652±0.037	126.40	1.76±0.10	−0.348±0.051
90.74	1.259±0.064	−0.420±0041			
97.88	1.224±0.061	−0.228±0.045			
106.72	1.586±0.077	−0.058±0.044			
115.32	1.503±0.073	−0.010±0.046			
123.64	1.228±0.058	0.008±0.043			
131.75	1.013±0.049	−0.020±0.046			

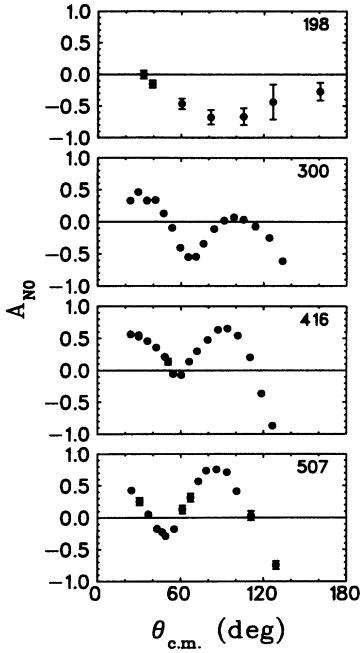

FIG. 6. Analyzing powers for the ^{3}He$(\vec{p},\pi^+)^4$He reaction. The data at 198 MeV are from Kehayias *et al.* [12]. The errors bars comprising the statistical and relative uncertainties added in quadrature are typically ± 0.04. In addition, there is an overall systematic error, not shown, of $\pm 2\%$.

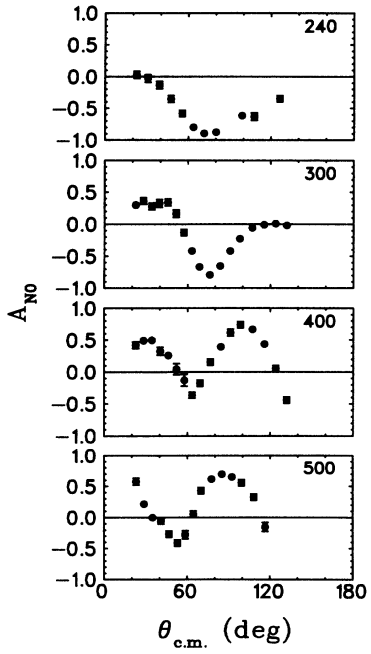

FIG. 7. Analyzing powers for the ^{4}He$(\vec{p},\pi^+)^5$He reaction. The errors bars comprising the statistical and relative uncertainties added in quadrature are typically ± 0.04. In addition, there is an overall systematic error, not shown, of $\pm 2\%$.

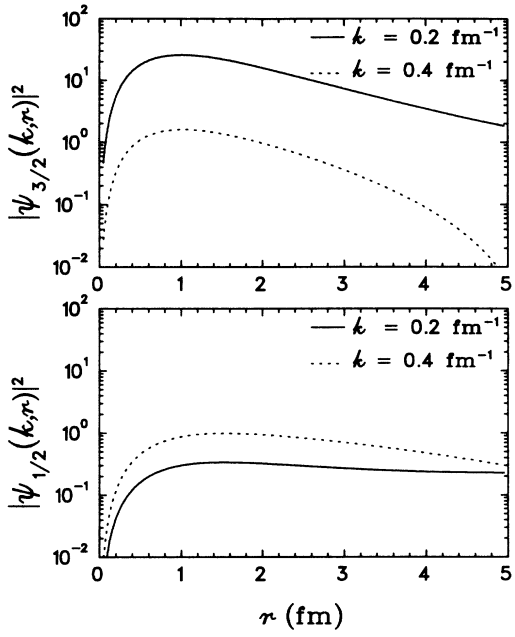

FIG. 8. Wave functions for the $P_{3/2}$ and $P_{1/2}$ states of ^{5}He. k and r are the relative momentum and space coordinates, respectively.

The enhancement factor is often equated with the modulus squared of the wave function at some constant radius (approximately the interaction distance) [34]. Here we assumed the enhancement to be of the form

$$|\zeta(k)|^2 = \int_{r_1}^{r_2} |\psi(k,r)|^2 r^2 dr,$$

where r_1 and r_2 were taken to be 0 and 2.0 fm, respectively. The enhancement calculated in this way is shown in Fig. 9 plotted versus the excitation energy.

The FSI spectra obtained from multiplying the phase space and enhancement factors were convoluted with a

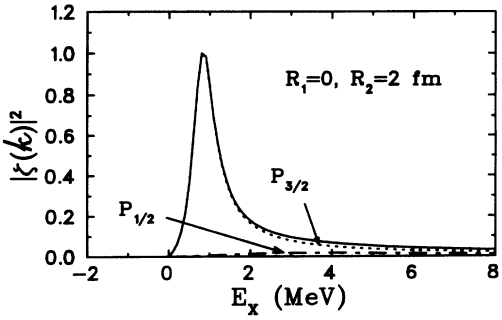

FIG. 9. Enhancement factor, $|\zeta(k)|^2$, the modulus of the wave function integrated from 0 to 2 fm. The dotted and dashed curves show the $P_{3/2}$ and $P_{1/2}$ state contributions, respectively, and the solid line the total.

Gaussian function to include effects of the experimental resolution, (typically $\sigma \approx 0.5$ MeV). The resulting FSI results are compared with several energies and angles in Fig. 10. One observes that the calculation fits the data well at the forward angles but departure from the data is observed for the back angles. Since the enhancement depends only on the excitation energy, the dependence of the FSI spectra on pion angle and proton energy arises solely from the phase space factor. However, the first quotient in the expression for the differential phase space, p_π^2/E_π, varies only slowly with excitation energy for a given proton energy and pion angle. Therefore, the predicted FSI spectra are a function of E_x alone, nearly independent of proton energy and pion angle. An underlying assumption in this analysis is that the transition matrix element does not depend on these other factors. The increasing discrepancy between the FSI predictions and the experimental spectra as the momentum transfer is increased reveals the limitations of these assumptions.

The total cross section attributable to the $n + \alpha$ $P_{3/2}$ state is difficult to determine, both for experimental and theoretical reasons. FSI spectra were integrated up to 4.44 MeV excitation and up to high excitation ($\approx$ 30 MeV), and from these results it was estimated that the former integration represented $60 \pm 10\%$ of the $P_{1/2}$ contribution. Within this interval up to 4.44 MeV the $P_{1/2}$ contribution is only about 7% of the $P_{3/2}$ contribution. Cross sections given for this reaction in Fig. 5 and in Table II represent the combined yield up to 4.44 MeV excitation.

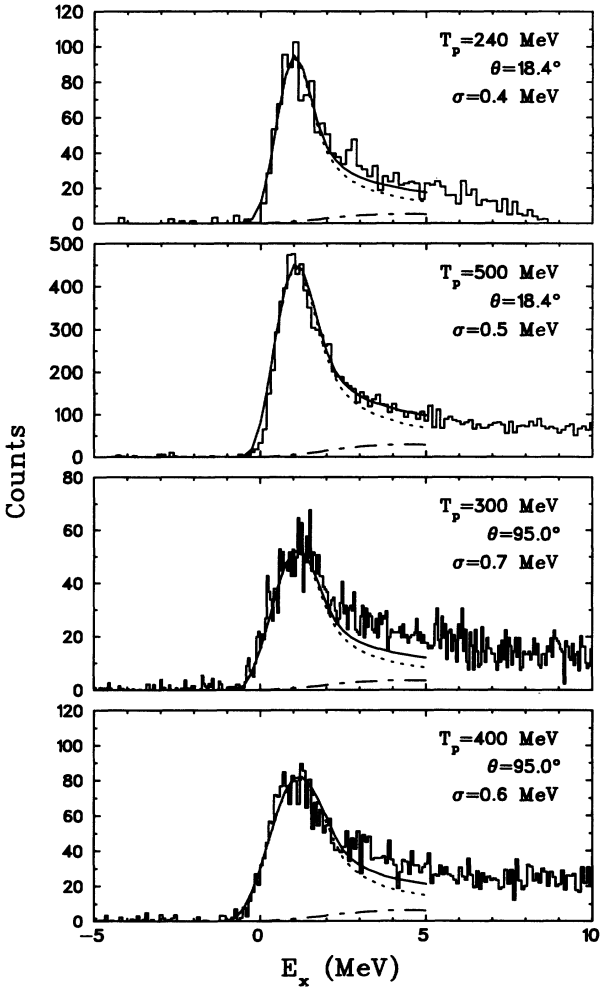

FIG. 10. Comparison of the final-state interaction calculation with the experimental spectra at several angles and energies. The dotted and dashed curves show the $P_{3/2}$ and $P_{1/2}$ state contributions, respectively, and the solid line the total.

V. RESULTS AND DISCUSSION

The differential cross sections for the two reactions, shown in Figs. 4 and 5, are very similar. They are quite flat close to threshold, and as the proton bombarding energy increases the cross sections become exponential in character. Interestingly, it is observed that the cross section for the ^{4}He$(p,\pi^+)^5$He reaction is larger in magnitude than that for the ^{3}He$(p,\pi^+)^4$He reaction despite the 4.44 MeV integration limit used in the former reaction. Moreover, it is observed that the analyzing powers, which are shown in Figs. 6 and 7, are also quite similar for the two reactions. Close to threshold, they have features very similar to the low energy $pp \rightarrow d\pi^+$ analyzing powers, and for proton energies at 300 MeV and above, large and rapid oscillations are observed. Corresponding to these oscillations in A_{N0}, the differential cross sections exhibit minima or inflections at $\theta_{\text{c.m.}} \approx 60°$.

Limited measurements of the ^{3}He$(\vec{p},\pi^+)^4$He and ^{4}He$(\vec{p},\pi^+)^5$He reaction cross sections have been made previously. A measurement by Tatischeff *et al.* [15] of the ^{3}He$(p,\pi^+)^4$He reaction at 415 MeV is compared to the 416 MeV data of this work in Fig. 11. While the results of Tatischeff are observed to be in fair agreement

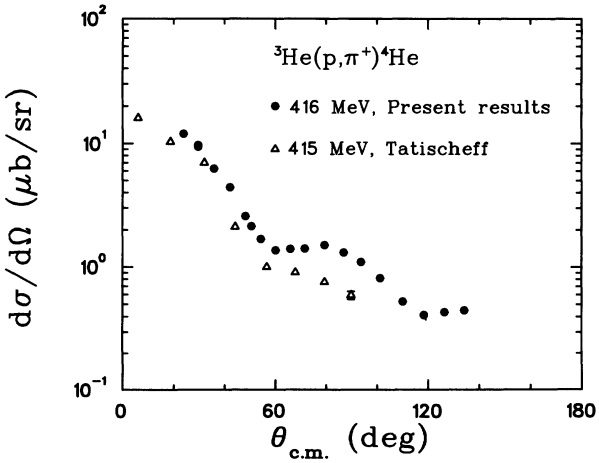

FIG. 11. Comparison of ^{3}He$(p,\pi^+)^4$He data from Tatischeff *et al.* [15] at 415 MeV with measurements of this work at 416 MeV.

in the forward region, the structure at $\theta_{\text{c.m.}} \approx 90°$ is not as evident as observed in the present measurement. Le Bornec *et al.* [14] measured the $^4\text{He}(p,\pi^+)^5\text{He}$ cross section at 200 MeV; the 240 MeV data of this work are found to be larger at the forward angles and approximately the same at the back angles (see Fig. 5). The measurement by Höistad *et al.* [16] at $T_p = 800$ MeV is too high in energy to allow comparison with the present data.

In Fig. 12 the $^3\text{He}(p,\pi^+)^4\text{He}$, $^4\text{He}(p,\pi^+)^5\text{He}$ and $pp \rightarrow d\pi^+$ cross sections are plotted versus $E_{\text{c.m.}} - m_{\text{target}}$ at a fixed momentum transfer, $|t| = 0.5$ GeV$^2/c^2$. The data are scaled arbitrarily to facilitate the comparison. The cross sections are observed to rise dramatically at approximately 1200 MeV which is evidence of a Δ_{1232} pole in the pion production reaction mechanism. Unlike the $pp \rightarrow d\pi^+$ reaction, the other reactions drop off only slowly with further increase in energy due to the additional $pN \rightarrow NN\pi^+$ channels available to the $A(p,\pi^+)A+1$ reactions.

The data were compared with the predictions of two models: a microscopic model, ORCHID [5]; and a $pp \rightarrow d\pi^+$ phenomenological model (described in [35]). ORCHID calculations were performed for the $^3\text{He}(\vec{p},\pi^+)^4\text{He}$ reaction at 178 and 198 MeV [5,36] and reasonably good agreement between experiment and theory was found. In Fig. 13 the results of a calculation at 300 MeV [37] are compared to the data of this work. As noted previously [35], for the forward angles of the analyzing power, ORCHID predicts the incorrect sign; however the calculation does reflect the change of character observed between 198 and 300 MeV. Bent *et al.* [36,37] performed detailed investigations with the ORCHID model which indicate that a significant part of the cross section at back angles originates from one nucleon pion production with momentum sharing from proton and nonresonant pion distortions. This is also found to some degree in the Δ-hole model calculations of Sakamoto *et al.* [38]. The ORCHID model

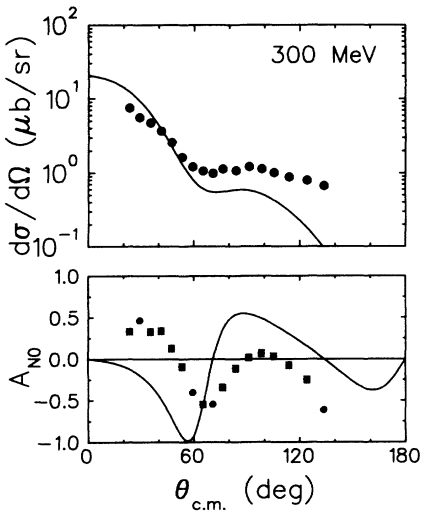

FIG. 13. Comparison of the microscopic ORCHID calculation (curve) for the $^3\text{He}(\vec{p},\pi^+)^4\text{He}$ reaction with the 300 MeV data of this work (points).

calculations indicate that there are substantial Coulomb effects [36], and furthermore that the effects depend on pion angle as well as beam energy.

Cross section data at an equivalent neutron bombarding energy for the time reversed charge symmetric reaction, $^3\text{H}(n,\pi^-)^4\text{He}$, by Källne *et al.* [39] are comparable to the Tatischeff *et al.* data [15] for $^3\text{He}(p,\pi^+)^4\text{He}$. However, the present measurements together with the data from Kehayias *et al.* [12] for the $^3\text{He}(p,\pi^+)^4\text{He}$ reaction and Källne *et al.* [39–41] for the $^4\text{He}(\pi^+,p)^3\text{He}$ reaction indicate that the (p,π^+) cross section is larger than the (n,π^-) cross section by factors up to 6 depending on beam energy. In Fig. 14 the cross sections are plotted versus energy at a single angle ($\theta_{\text{c.m.}} \approx 22°$). One observes

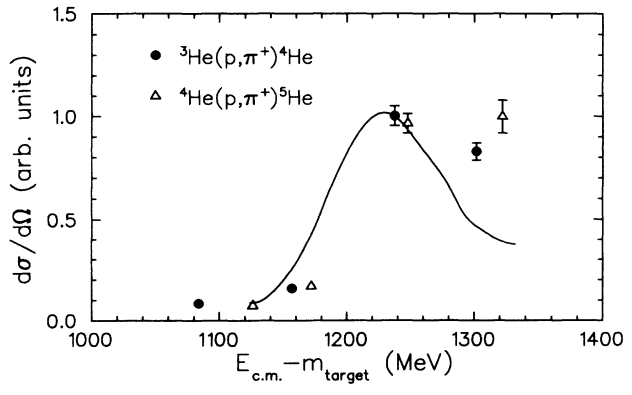

FIG. 12. Comparison of $^3\text{He}(p,\pi^+)^4\text{He}$, $^4\text{He}(p,\pi^+)^5\text{He}$ and $pp \rightarrow d\pi^+$ (solid line) differential cross sections as a function of $E_{\text{c.m.}} - m_{\text{target}}$ (MeV) at a constant momentum transfer of $|t| = 0.5$ GeV$^2/c^2$. The cross sections have been rescaled to emphasize the comparison.

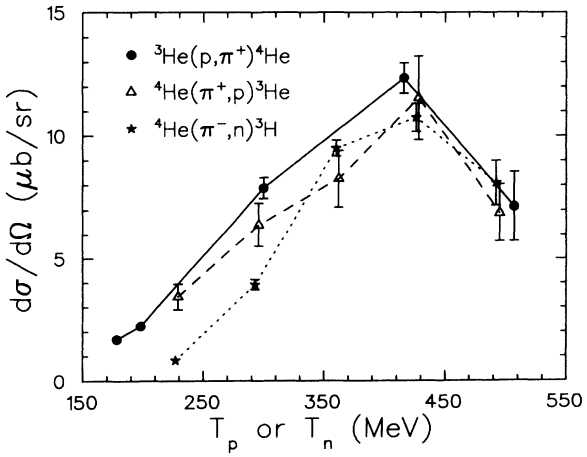

FIG. 14. Comparison of energy dependence of $^3\text{He}(p,\pi^+)^4\text{He}$ and $^3\text{He}(n,\pi^-)^4\text{He}$ reactions at $\theta_{\text{c.m.}} \approx 22°$. Lines connecting the data points have been drawn to guide the eye.

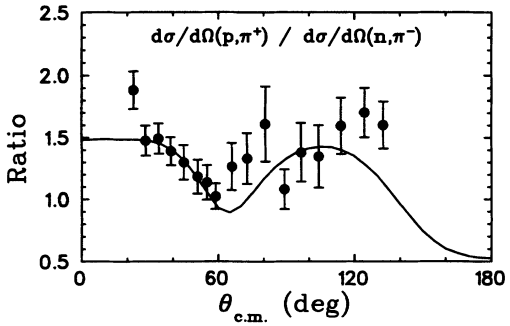

FIG. 15. The ratio of the ^{3}He$(p,\pi^+)^4$He to the ^{3}H$(n,\pi^-)^4$He cross sections as a function of angle at $T_p = 300$ MeV (points). The curve is the prediction of the ORCHID calculation.

that Coulomb effects are substantial near threshold and then decrease with increasing beam energy. Figure 15 shows the ratio of the ^{3}He$(p,\pi^+)^4$He and ^{3}H$(n,\pi^-)^4$He cross sections as a function of angle at $T_p = 300$ MeV ($T_\pi = 100$ MeV). Also, shown is the result from the ORCHID calculation [37], which describes the experimentally observed ratio rather well.

Detailed calculations of the differential cross sections and analyzing powers were also carried out for the ^{3}He$(\vec{p},\pi^+)^4$He reaction using the $pp \rightarrow d\pi^+$ model discussed briefly in [35]. Results at several energies in the neighborhood of 300 MeV using this model are shown in Fig. 16. These energies were chosen to indicate the sensitivity of the results, particularly the analyzing powers, to the incident beam energy. Figure 16 indicates that the shape of the differential cross sections is very well reproduced. (The absolute magnitude is not very well defined in this model, and the calculated results were each multiplied by a factor of 1.1 before plotting.) The analyzing powers are also well reproduced in general form, if not in all details. It is important to emphasize that the shapes of the indicated analyzing powers are only obtained if a D-state component is included for the ^{3}He target wave function. The effect of setting the D-state component to zero results in the calculation shown by the dotted curve. Earlier calculations [35] assumed S state only for ^{3}He.

Surprisingly, whereas the ORCHID calculation finds the two nucleon mechanism alone insufficient to describe the back angle region of the 300 MeV cross sections [36], the $pp \rightarrow d\pi^+$ model describes it rather well. Details of the investigations of the ^{3,4}He$(\vec{p},\pi^+)^{4,5}$He and ^{12}C$(\vec{p},\pi^+)^{13}$C reactions with the $pp \rightarrow d\pi^+$ model will be presented in a forthcoming publication [10].

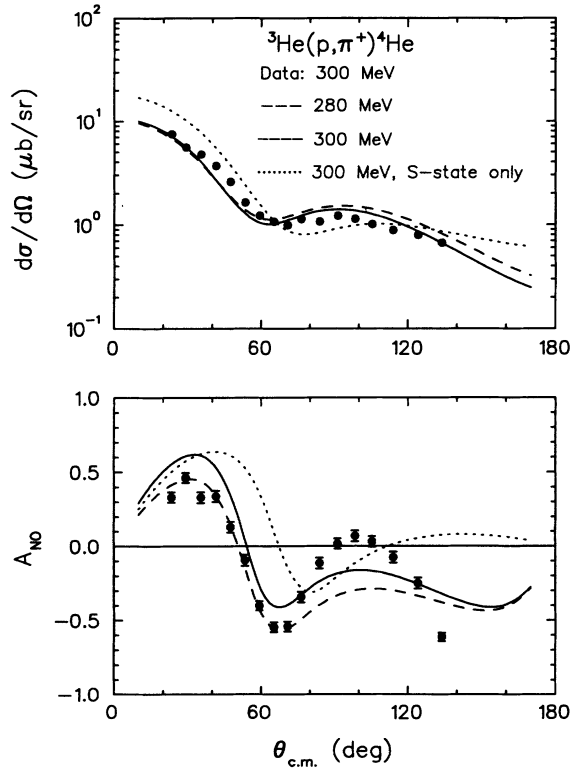

FIG. 16. Comparison of a phenomenological $pp \rightarrow d\pi^+$ model calculation (curve) for the ^{3}He$(\vec{p},\pi^+)^4$He reaction with the 300 MeV data of this work (points). The dotted curve is obtained if no D state is included in the ^{3}He wave function.

VI. CONCLUSION

Angular distributions of the differential cross sections and analyzing powers have been measured for the ^{3}He$(\vec{p},\pi^+)^4$He and ^{4}He$(\vec{p},\pi^+)^5$He reactions at proton bombarding energies between 240 and 507 MeV. These new results provide a comprehensive set of data for few nucleon systems spanning the region of the Δ_{1232} resonance where the underlying $NN \rightarrow N\Delta \rightarrow NN\pi^+$ processes dominate. Evidence of an underlying Δ_{1232} mechanism is clearly observed in the cross section energy dependence as shown in Fig. 12.

A ^{5}He final state interaction calculation based upon the low-energy $n + \alpha$ elastic phase shifts indicates that the ^{4}He$(p,\pi^+)^5$He spectra are nearly independent of pion angle and proton energy. In addition, despite a 4.44 MeV upper integration limit, the ^{4}He$(p,\pi^+)^5$He cross section is observed to be larger in magnitude than the ^{3}He$(p,\pi^+)^4$He cross section. The shape of the cross sections and analyzing powers are very similar for the ^{3}He$(\vec{p},\pi^+)^4$He and ^{4}He$(\vec{p},\pi^+)^5$He reactions indicating a strong similarity in the underlying reaction mechanism, independent of the spin details of the target and residual nuclei.

The ^{3}He$(\vec{p},\pi^+)^4$He calculations using the microscopic (p,π^+) model reflect some of the structure observed in the angular distributions of both the differential cross sections and analyzing powers. Indeed, Coulomb effects, which are predicted in the microscopic model, are also found from a comparison of the ^{3}He$(p,\pi^+)^4$He reaction measurements of this work to previous ^{3}H$(n,\pi^-)^4$He re-

action data, as shown in Fig. 15. A phenomenological $pp \rightarrow d\pi^+$ model is in good agreement with the data at 300 MeV if a D-state component is included in the ^{3}He target wave function. This level of agreement places the supposition that exclusive (p,π^+) reactions are mediated by the elementary $pp \rightarrow d\pi^+$ reaction on a much sounder footing. Moreover, this simple model provides useful insights which are easily lost in the complex microscopic calculations. Nevertheless, there is a real need to further develop microscopic models to improve our understanding of these reactions.

ACKNOWLEDGMENTS

The authors would like to thank the TRIUMF staff for their help during the preparation and running of the experiment, especially C. A. Miller for his assistance in operation of the MRS. In particular K.F., W.F., and F.D. wish to express their appreciation to R. Abegg and D. C. Healy and the TRIUMF technicians for their advice and assistance with refurbishing of the liquid ^{3}He target. This work has been supported in part by the Natural Sciences and Engineering Research Council of Canada (NSERC).

[1] S. Dahlgren, B. Höistad, and P. Grafstrom, Phys. Lett. **35B**, 219 (1971).
[2] H. W. Fearing, Prog. Part. Nucl. Phys. **7**, 113 (1981); B. Höistad, Adv. Nucl. Phys. **11**, 135 (1979); D. F. Measday and G. A. Miller, Annu. Rev. Nucl. Sci. **29**, 121 (1979).
[3] *Pion Production and Absorption in Nuclei-1981 (Indiana University Cyclotron Facility)*, Proceedings of the Conference on Pion Production and Absorption in Nuclei, edited by R. D. Bent, AIP Conf. Proc. No. 79 (AIP, New York, 1982).
[4] See, for example, E. D. Cooper and H. S. Sherif, Phys. Rev. C **25**, 3024 (1982); M. J. Iqbal and G. E. Walker, *ibid.* **32**, 557 (1985); B. D. Keister and L. S. Kisslinger, Nucl. Phys. **A412**, 301 (1984).
[5] P. W. F. Alons, R. D. Bent, J. S. Conte, and M. Dillig, Nucl. Phys. **A480**, 413 (1988); P. W. F. Alons, R. D. Bent, and M. Dillig, *ibid.* **A493**, 509 (1989).
[6] See, for example, E. G. Auld *et al.*, Phys. Rev. Lett. **41**, 462 (1978); T. P. Sjoreen *et al.*, Phys. Rev. C **24**, 1135 (1981); and Korkmaz *et al.*, *ibid.* **40**, 813 (1989).
[7] E. Korkmaz, Ph.D. thesis, University of Indiana, 1987.
[8] G. M. Huber, Ph.D. thesis, University of Regina, 1988.
[9] D. Kurath, Phys. Rev. C **35**, 2247 (1987).
[10] W. R. Falk, Phys. Rev. C **50**, 1574 (1994).
[11] K. M Furutani, Ph.D. thesis, University of Manitoba, 1992.
[12] J. J. Kehayias, R. D. Bent, M. C. Green, M. A. Pickar, and R. E. Pollock, Phys. Rev. C **33**, 725 (1986).
[13] N. Willis, L. Bimbot, N. Koori, Y. LeBornec, F. Reide, A. Willis, and C. Wilkin, J. Phys. G: Nucl. Phys. **7**, L195 (1981).
[14] Y. LeBornec, L. Bimbot, M. P. Combes-Comets, J. C. Jourdain, F. Reide, A. Willis, and N. Willis, J. Phys. G: Nucl. Phys. **11**, 1125 (1985).
[15] B. Tatischeff, L. Bimbot, R. Frascaria, Y. LeBornec, M. Morlet, N. Willis, R. Beurtey, G. Bruge, P. Couvert, D. Garreta, D. Legrand, G. A. Moss, and Y. Terrien, Phys. Lett. **63B**, 158 (1976).
[16] B. Höistad, M. Gazzaly, B. Aas, G. Igo, A. Rahbar, C. Whitten, G. S. Adams, and R. Whitney, Phys. Rev. C **29**, 553 (1984).
[17] Yu. K. Akimov, O. V. Savchenko, and L. M. Soroko, Zh. Eksp. Teor. Fiz. **41**, 708 (1961) [Sov. Phys. JETP **14**, 512 (1962)]; K. Gabathuler, J. Rohlin, J. J. Domingo, C. H. Q. Ingram, S. Rohlin, and N. W. Tanner, Nucl. Phys. **B40**, 32 (1972).
[18] R. A. Arndt and D. Roper, VPI and SU Scattering Analysis Interactive Dial-In Program and Data Base, 1989.
[19] D. K. Hasell, R. Abegg, B. T. Murdoch, W. T. H. van Oers, H. Postma, and J. Soukup, Nucl. Instrum. Methods **189**, 341 (1981).
[20] LakeShore Cryotonics, Inc., Westerville, Ohio.
[21] B. Coyler, *Cryogenic Properties of Helium-3 and Helium-4*, Central Engineering Group, Rutherford High Energy Laboratory (Chilton Didcot, Berkshire, 1966).
[22] D. K. Hasell, A. Bracco, H. P. Gubler, W. P. Lee, W. T. H. van Oers, R. Abegg, D. A. Hutcheon, C. A. Miller, J. M. Cameron, L. G. Greeniaus, G. A. Moss, M. P. Epstein, and D. J. Margaziotis, Phys. Rev. C **34**, 236 (1986).
[23] G. A. Moss, L. G. Greeniaus, J. M. Cameron, D. A. Hutcheon, R. L. Liljestrand, C. A. Miller, G. Roy, B. K. S. Koene, W. T. H. van Oers, A. W. Stetz, A. Willis, and N. Willis, Phys. Rev. C **21**, 1932 (1980).
[24] C. A. Miller, in *Proceedings of the Workshop on Studying Nuclei with Medium Energy Protons*, Edmonton, Alberta, Canada, 1983, edited by J. M. Greben (TRIUMF Proceedings TRI-83-3, 339 (1983).
[25] S. Yen, Nucl. Instrum. Methods Phys. Res. Sect. A **302**, 493 (1991).
[26] G. M. Huber, G. J. Lolos, K. M. Furutani, W. R. Falk, R. D. Bent, K. H. Hicks, P. L. Walden, and S. Yen, Phys. Rev. C **38**, 1304 (1988), and references therein.
[27] J. F. Crawford, M. Daum, G. H. Eaton, R. Frosch, H. Hirschmann, R. Horisberger, J. W. McCulloch, E. Steiner, R. Hausammann, R. Hess, and D. Werren, Phys. Rev. C. **22**, 1184 (1980).
[28] V. A. Krasnov, A. B. Kurepin, A. I. Reshetin, K. O. Oganesjan, and E. A. Pasyuk, Phys. Lett. **108B**, 11 (1982).
[29] *Proceedings of the Higher Energy Polarized Proton Beams-1977, Ann Arbor, Michigan*, edited by A. D. Krisch and A. J. Salthouse, AIP Conf. Proc. No. 42 (AIP, New York, 1978).
[30] *Proceedings of the 3rd International Symposium on Polarization Phenomena in Nuclear Reactions, Madison, Wisconsin, 1970*, edited by H. H. Barschall and W. Haeberli (University of Wisconsin, Madison, 1971).
[31] J. E. Bond and F. W. K. Firk, Nucl. Phys. **A287**, 317 (1977).
[32] J. F. Germond and C. Wilkin, J. Phys. G: Nucl. Phys. **11**, 1131 (1985).
[33] R. Hagedorn, *Relativistic Kinematics* (Benjamin, New York, 1963).
[34] G. F. Wolters, in *Final State Interactions in Kinematics and Multiparticle Systems*, edited by M. Nikolić for the Proceedings of the International School of Elementary

Particle Physics (Gordon and Breach, New York, 1968), pp. 267–313.
[35] K. M. Furutani, W. R. Falk, F. A. Duncan, P. L. Walden, S. Yen, G. M. Huber, R. D. Bent, G. J. Lolos, and E. Korkmaz, Phys. Rev. C **44**, 1691 (1991).
[36] R. D. Bent, P. W. F. Alons, and M. Dillig, Nucl. Phys. **A511**, 541 (1990).
[37] R. D. Bent, unpublished.
[38] K. Sakamoto, M. Hirata, A. Matsuyama, and K. Yazaki, Phys. Rev. C **31**, 1987 (1985).
[39] J. Källne, H. A. Thiessen, C. L. Morris, S. L. Verbeck, G. R. Burleson, M. J. Devereaux, J. S. McCarthy, J. E. Bolger, C. F. Moore, and C. A. Goulding, Phys. Rev. Lett. **40**, 378 (1978).
[40] J. Källne, J. E. Bolger, M. J. Devereaux, and S. L. Verbeck, Phys. Rev. C **24**, 1102 (1981).
[41] J. Källne, R. C. Minehart, R. R. Whitney, R. L. Boudrie, J. B. McClelland, and A. W. Stetz, Phys. Rev. C **28**, 304 (1983).